

See discussions, stats, and author profiles for this publication at: <https://www.researchgate.net/publication/223549389>

Synthesis and Mechanistic Studies of Organic Chromophores with Different Energy Levels for p-Type Dye–Sensitized Solar Cells

ARTICLE · FEBRUARY 2010

DOI: 10.1021/jp911091n

CITATIONS

74

READS

37

9 AUTHORS, INCLUDING:



Peng Qin

École Polytechnique Fédérale de Lausanne

18 PUBLICATIONS 1,453 CITATIONS

[SEE PROFILE](#)



Mats Linder

KTH Royal Institute of Technology

14 PUBLICATIONS 351 CITATIONS

[SEE PROFILE](#)



Tore Brinck

KTH Royal Institute of Technology

129 PUBLICATIONS 4,121 CITATIONS

[SEE PROFILE](#)



Bo Albinsson

Chalmers University of Technology

135 PUBLICATIONS 4,589 CITATIONS

[SEE PROFILE](#)

Synthesis and Mechanistic Studies of Organic Chromophores with Different Energy Levels for p-Type Dye-Sensitized Solar Cells

Peng Qin,[†] Joanna Wiberg,[‡] Elizabeth A. Gibson,[§] Mats Linder,[†] Lin Li,[†] Tore Brinck,[†] Anders Hagfeldt,^{§,⊥} Bo Albinsson,[‡] and Licheng Sun^{*,†,⊥}

Center of Molecular Devices, Department of Chemistry, School of Chemical Science and Engineering, Royal Institute of Technology (KTH), 100 44 Stockholm, Sweden, Department of Chemical and Biological Engineering/Physical Chemistry, Chalmers University of Technology, 412 96 Göteborg, Sweden, Department of Physical and Analytical Chemistry, Uppsala University, Box 259, 751 05 Uppsala, Sweden, and DUT-KTH Joint Research Center on Molecular Devices, State Key Laboratory of Fine Chemicals, Dalian University of Technology (DUT), 116012 Dalian, China

Received: November 22, 2009; Revised Manuscript Received: January 28, 2010

A series of donor- π -acceptor dyes with different electron-withdrawing groups were designed and synthesized for p-type dye-sensitized solar cells. The modification of dye structures shows significant influence on the photophysical, electrochemical, and photovoltaic performance of the dyes. DSSCs based on these dyes show maximum 63% and minimum 6% of incident monochromatic photon-to-current conversion efficiencies. The two dyes with the highest (**P1**) and lowest (**P3**) efficiencies were studied by femtosecond transient absorption spectroscopy, which shows a fast injection rate of more than $(250 \text{ fs})^{-1}$ for both dyes. Such fast injection corresponds to more than 90% injection efficiency. The photoinduced absorption spectroscopy study of sensitized NiO films in the presence of electrolyte showed poor regeneration of **P3** due to an insufficient driving force. This, together with aggregation of the dye on the NiO film, explained the poor solar cell performance.

Introduction

Dye-sensitized solar cells with photoactive cathodes (p-type DSSCs) have recently attracted much attention due to the development of new materials and sensitizers.^{1–8} Dye sensitization of the photocathode occurs by a hole injection mechanism, from the photoexcited dye to the semiconductor. Although the reported efficiencies for p-type DSSCs are much lower than those of the Grätzel type solar cells (n-type DSSCs),^{9–12} the investigation of this system is useful to identify the parameters governing the efficiency from a fundamental viewpoint, which is important for the rational design of more efficient photovoltaic devices based on this principle in the future.

The p-type semiconductor used in our work is NiO, which has a band gap of ~ 3.5 eV and has the advantage of good stability and transparency. The generation of cathodic photocurrent in NiO based solar cells has been reported using several different dyes, such as triphenylamine based chromophores,^{4,5} coumarin,^{1,3,13–15} peryleneimide,^{2,6} erythrosin,^{16,17} and porphyrin.^{17,18} To be a good sensitizer, the energy levels of a dye should match well with the energy of the valence band of the semiconductor and the redox potential of the electrolyte, providing sufficient driving force for hole injection and dye regeneration. Long-lived charge-separated state and avoidance of aggregation are also preferable to achieve higher efficiency.

We have shown in our previous studies a successful model for the design of efficient dyes for p-type DSSCs.^{4,5} Here we will pay more attention to the influence of energy levels of the dye on the photovoltaic performance of the solar cells. Specif-

ically, we have compared the effect of varying the electron-withdrawing groups on the individual electron transfer reactions in the system and the corresponding photovoltaic performance of the device. We hope that this will enable us to direct our approach to the design of optimized dyes for p-type DSSCs in the future. Therefore, we have designed and synthesized a series of organic chromophores, 4-(bis[4-[5-(1,3-diethyl-4,6-dioxo-2-thioxotetrahydropyrimidin-5-ylidenemethyl)thiophen-2-yl]phenyl]amino)benzoic acid (**P2**), 4-[bis[4-(5-tricyanovinylthiophen-2-yl)phenyl]amino]benzoic acid (**P3**), and 4-[bis(4-[5-[2-(3-dicyanomethylene-5,5-dimethylcyclohex-1-enyl)vinyl]thiophen-2-yl]phenyl)amino]benzoic acid (**P7**). For comparison, **P1**, one of the most efficient dyes used in our earlier studies of p-type systems, has also been included (Figure 1). In this paper, we report the synthesis, characterization, photovoltaic properties, and ultrafast dynamic studies of these dyes used in p-type DSSCs.

Experimental Section

Analytical Measurements. NMR spectra were measured on a Bruker AVANCE 500 MHz spectrometer, using TMS as internal standard. High-resolution mass spectrometry (HRMS) was performed by using a Q-ToF Micro mass spectrometer equipped with a Z-spray ionization source. UV-vis absorption and emission spectra were recorded on a Lambda 750 UV-vis spectrometer and a Cary Eclipse fluorescence spectrophotometer, respectively. Cyclic voltammetry was performed with a CH Instruments 660 potentiostat using 0.1 M tetrabutylammonium hexafluorophosphate TBA(PF₆) as supporting electrolyte. A glass carbon working electrode, platinum counter electrode, and Ag/Ag⁺ reference electrode were used. The system was calibrated with ferrocene/ferrocenium (Fc/Fc⁺). Samples for infrared absorption spectroscopy were prepared as KBr pressed

* To whom correspondence should be addressed. E-mail: lichengs@kth.se.

[†] Royal Institute of Technology.

[‡] Chalmers University of Technology.

[§] Uppsala University.

[⊥] Dalian University of Technology.

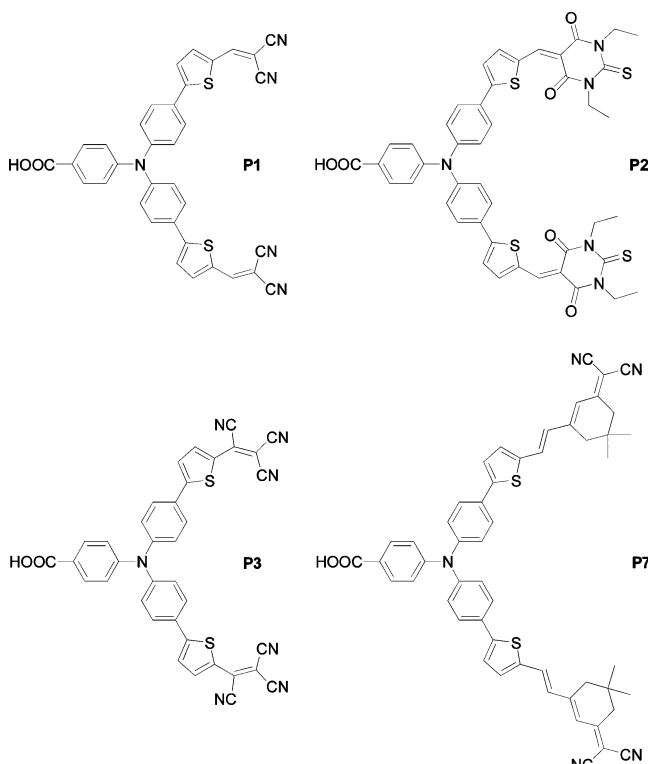


Figure 1. Molecular structures of **P1**, **P2**, **P3**, and **P7**.

disks, and spectra were recorded for 16 scans between 500 and 5000 cm^{-1} at a resolution of 2 cm^{-1} with a Bruker FT-IR spectrometer (IFS 66v/S).

Incident photon-to-current conversion efficiencies were recorded using a monochromatic light from a system consisting of a xenon lamp, a monochromator, and appropriate filters. $I-V$ characteristics were measured using a Keithley source/meter under simulated sunlight from a Newport 300 W solar simulator, giving light with an intensity of 100 mW cm^{-2} . Both systems were calibrated against a certified reference solar cell (IR-filtered silicon solar cell, Fraunhofer ISE, Freiburg, Germany).

Spectroelectrochemical measurements were performed either on films—NiO films on FTO sensitized with **P1** and **P3**—or in solution—0.01 M dye dissolved in the supporting electrolyte with a platinum grid working electrode. The supporting electrolyte for both measurements was 0.1 M LiClO_4 in acetonitrile, which was degassed by bubbling with nitrogen. The reference electrode was Ag/Ag^+ in acetonitrile, and the counter electrode was a Pt wire.

The femtosecond setup has been described in detail elsewhere.¹⁹ The samples were either sensitized NiO films with a drop of 1 M LiClO_4 in acetonitrile or dyes dissolved in solution directly. The probe and reference beams were after passing the sample focused on optical fibers connected to a spectrograph (Shamrock sr-303i, Andor) and detected at 1 kHz by a CCD camera (iXon em⁺, Andor). Between 200 and 1000 scans were averaged for each delay time depending on signal amplitude. The group velocity dispersion of the probe white light was fitted to a third-order polynomial and corrected for by use of a homemade MATLAB program.

4-(Bis{4-[5-(1,3-diethyl-4,6-dioxo-2-thioxotetrahydropyrimidin-5-ylidenemethyl)thiophen-2-yl] phenyl]amino)benzoic acid (P2**).** A mixture of compound **1** (0.12 mmol, 61.2 mg) and 1,3-diethyl-2-thiobarbituric acid (0.36 mmol, 72.1 mg) in acetic anhydride (1.5 mL) was stirred at 120 °C for 4 h under N_2 atmosphere. After cooling to room temperature, dichloromethane

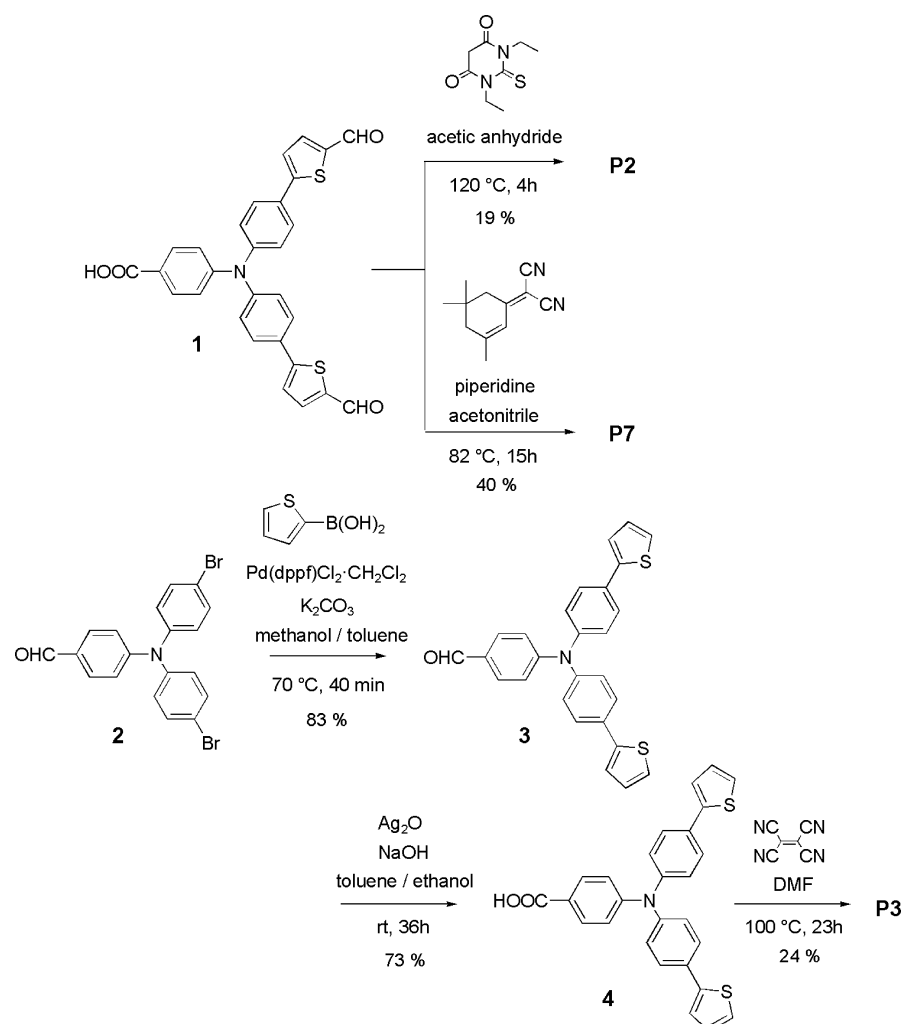
(DCM) (80 mL) was added. The mixture was washed with 5% NaHCO_3 aqueous (3×100 mL) and dried with anhydrous sodium sulfate. After solvent removal, the residue was purified by column chromatography on silica gel using an acetone/petroleum ether mixture as the eluent to give the product (20 mg, 19%) as a dark red solid. mp 253–255 °C. ^1H NMR (400 MHz, THF, ppm): δ 1.26 (m, 12H), 4.56 (m, 8H), 7.20 (d, J = 8.8 Hz, 2H), 7.24 (d, J = 8.8 Hz, 4H), 7.67 (d, J = 4.4 Hz, 2H), 7.87 (d, J = 8.4 Hz, 4H), 7.96 (d, J = 8.4 Hz, 2H), 8.06 (d, J = 4.4 Hz, 2H), 8.66 (s, 2H), 11.30 (s, 1H). ^{13}C NMR (125 MHz, THF, ppm): δ 12.6, 12.7, 43.5, 44.2, 111.6, 123.9, 125.4, 126.0, 128.8, 130.1, 132.1, 137.6, 148.3, 148.9, 149.1, 151.2, 160.7, 160.7, 161.4, 167.0, 180.0. HRMS-ESI m/z ([M – H][–]): calcd for $\text{C}_{45}\text{H}_{39}\text{N}_5\text{O}_6\text{S}_4$ 872.1705, found 872.1728.

4-[Bis{4-[5-[2-(3-dicyanomethylene-5,5-dimethylcyclohex-1-enyl)vinyl]thiophen-2-yl]phenyl]amino]benzoic acid (P7**).** To a solution of compound **1** (0.10 mmol, 51.0 mg) in acetonitrile (40 mL) were added 2-(3,5,5-trimethylcyclohex-2-enylidene)malononitrile (0.40 mmol, 74.5 mg) and piperidine (5 μL). The mixture was refluxed at 82 °C for 15 h. After cooling to room temperature, water (5 mL) was added. The mixture was extracted with ethyl acetate (3×60 mL) and dried with anhydrous sodium sulfate. After solvent removal, the residue was purified by column chromatography on silica gel using a pentane/ethyl acetate mixture as the eluent to give the product (34 mg, 40%) as a dark red solid. mp 185–187 °C. ^1H NMR (500 MHz, $(\text{CD}_3)_2\text{CO}$, ppm): δ 1.11 (s, 12H), 2.61 (s, 4H), 2.67 (s, 4H), 6.88 (s, 2H), 7.09 (d, J = 15.7 Hz, 2H), 7.17 (d, J = 8.4 Hz, 2H), 7.24 (d, J = 8.3 Hz, 4H), 7.41 (d, J = 3.7 Hz, 2H), 7.51 (m, 4H), 7.73 (d, J = 8.3 Hz, 4H), 7.97 (d, J = 8.4 Hz, 2H). ^{13}C NMR (125 MHz, $(\text{CD}_3)_2\text{CO}$, ppm): δ 28.0, 32.6, 39.4, 43.4, 78.0, 113.7, 114.5, 122.7, 123.6, 125.1, 125.3, 126.5, 127.8, 129.4, 130.6, 131.2, 132.1, 132.7, 142.0, 146.8, 147.5, 151.9, 155.6, 167.1, 170.2. HRMS-ESI m/z ([M – H][–]): calcd for $\text{C}_{53}\text{H}_{43}\text{N}_5\text{O}_2\text{S}_2$ 844.2785, found 844.2796.

4-[Bis(4-thiophen-2-yl-phenyl)amino]benzaldehyde (3**).** To a solution of compound **2** (0.46 mmol, 200.0 mg) and $\text{Pd}(\text{dpf})\text{Cl}_2 \cdot \text{CH}_2\text{Cl}_2$ (0.05 mmol, 40.8 mg) in toluene (2.5 mL) was added a solution of 2-thiophene boronic acid (1.61 mmol, 206.1 mg) and K_2CO_3 (2.30 mmol, 317.4 mg) in methanol (2.5 mL). The mixture was heated by microwave oven irradiation at 70 °C for 40 min and then poured into a saturated solution of ammonium chloride (150 mL). Extracted with DCM (3×100 mL), the combined organic phases were washed with brine and dried over anhydrous sodium sulfate. After solvents were evaporated, the residue was purified by column chromatography on silica gel using a DCM/pentane mixture as the eluent to give the product (168 mg, 83%) as a light yellow solid. mp 85–87 °C. ^1H NMR (500 MHz, $(\text{CD}_3)_2\text{CO}$, ppm): δ 7.14 (m, 4H), 7.26 (d, J = 8.5 Hz, 4H), 7.46 (m, 4H), 7.72 (d, J = 8.5 Hz, 4H), 7.80 (d, J = 8.5 Hz, 2H), 9.88 (s, 1H). ^{13}C NMR (125 MHz, $(\text{CD}_3)_2\text{CO}$, ppm): δ 121.1, 124.2, 125.9, 127.3, 127.9, 129.2, 131.2, 131.9, 132.1, 144.2, 146.4, 153.5, 190.8. MS (ESI) m/z : 438.1 [M + H]⁺.

4-[Bis(4-thiophen-2-ylphenyl)amino]benzoic acid (4**).** Silver oxide (2.72 mmol, 631.0 mg) was suspended in ethanol (60 mL) containing sodium hydroxide (34.0 mmol, 1.4 g). To the solution was added compound **3** (0.68 mmol, 0.3 g) dissolved in toluene (2 mL). The mixture was stirred at room temperature for 36 h. The solution was then decanted and precooled HCl (10%, 50 mL) was added slowly. Extracted with ethyl acetate (3×100 mL), the organic phase was washed with water and dried with anhydrous sodium sulfate. It was filtered and the solvent was evaporated. The residue was purified by column

SCHEME 1: Synthetic Routes for P2, P3, and P7



chromatography on silica gel using an acetone/petroleum ether mixture as the eluent to give the product (225 mg, 73%) as a light yellow solid. mp 286–288 °C. ¹H NMR (500 MHz, DMSO, ppm): δ 7.02 (d, *J* = 8.5 Hz, 2H), 7.15 (m, 6H), 7.46 (d, *J* = 3.5 Hz, 2H), 7.52 (d, *J* = 5.0 Hz, 2H), 7.66 (d, *J* = 8.5 Hz, 4H), 7.83 (d, *J* = 8.5 Hz, 2H). ¹³C NMR (125 MHz, DMSO, ppm): δ 120.5, 123.5, 123.6, 125.5, 125.7, 126.9, 128.6, 130.0, 131.0, 142.8, 145.3, 150.6, 166.9. MS (ESI) *m/z*: 452.2 [M – H]⁻.

4-[Bis[4-(5-tricyanovinylthiophen-2-yl)phenyl]amino]benzoic acid (P3). A mixture of compound 4 (0.44 mmol, 0.2 g) and tetracyanoethylene (TCNE) (2.20 mmol, 281.8 mg) in 10 mL of anhydrous DMF was stirred at 100 °C for 23 h. The reaction mixture was poured into a saturated NaCl aqueous solution (150 mL) leading to the precipitation of a blue powder which was filtered, washed with water, washed with hexane, and then dried under vacuum. The powder was purified again by column chromatography on silica gel using an acetone/petroleum ether mixture as the eluent to give the product (69 mg, 24%) as a dark blue solid. mp 197–199 °C. ¹H NMR (500 MHz, THF, ppm): δ 7.24 (m, 6H), 7.74 (m, 2H), 7.83 (m, 4H), 7.98 (m, 2H), 8.13 (m, 2H), 11.37 (s, 1H). ¹³C NMR (125 MHz, THF, ppm): δ 84.0, 113.2, 113.5, 113.9, 124.7, 125.8, 126.3, 127.7, 128.3, 129.2, 132.2, 133.0, 133.4, 142.1, 149.7, 150.7, 158.2, 166.9. HRMS-ESI *m/z* ([M – H]⁻): calcd for C₃₇H₁₇N₇O₂S₂ 654.0807, found 654.0818.

Fabrication of Dye-Sensitized Solar Cells. NiO films (1.2 μm) were prepared by two cycles of doctor blading an F108-

templated precursor solution onto conducting glass substrates (Pilkington TEC8, sheet resistance 8 Ω/square), followed by sintering at 450 °C for 30 min (thickness was measured by a Sloan Dektak 3 profilometer).^{20,21} The prepared NiO electrodes were soaked in a 0.3 mM dye solution in acetonitrile (**P1** and **P7**) or THF (**P2** and **P3**) for 16 h at room temperature. The counter electrodes were prepared by coating the FTO plate with H₂PtCl₆ solution (5 mM in 2-propanol), followed by heating at 380 °C for 30 min. The dyed NiO electrode and Pt counter electrode were assembled into a sandwich-type cell using a 50 μm thick thermoplastic frame (Surlyn 1702) as spacer. A drop of electrolyte consisting of 1.0 M LiI and 0.1 M I₂ in acetonitrile was introduced through the predrilled hole in the counter electrode, which was sealed afterward. The cell had an active area of 0.32 cm².

Results and Discussion

I. Dye Design and Cell Performance. Synthesis. The synthetic routes of the dyes are shown in Scheme 1. **P1** and 4-[bis[4-(5-formylthiophen-2-yl)phenyl]amino]benzoic acid (**1**) were obtained as reported earlier.⁴ **P2** and **P7** were synthesized by the condensation of compound **1** with 1,3-diethyl-2-thiobarbituric acid and 2-(3,5,5-trimethylcyclohex-2-enylidene)-malononitrile, respectively.^{22,23} The synthesis of **P3** was based on the Suzuki coupling reaction of 4-[bis(4-bromophenyl)amino]benzaldehyde (**2**) with 2-thiophene boronic acid under microwave irradiation,²⁴ followed by oxidation reaction with

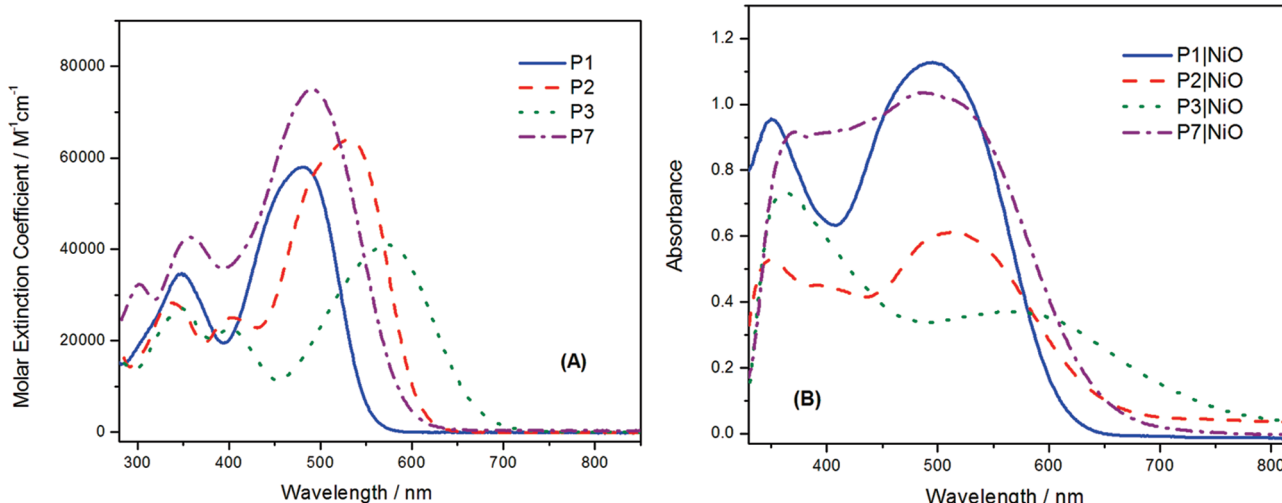


Figure 2. Absorption spectra of **P1**, **P2**, **P3**, and **P7** in THF solution (A) and adsorbed on NiO film (B).

TABLE 1: Optical and Electrochemical Properties of the Dyes

| dye | λ_{abs} ($M^{-1} \text{cm}^{-1}/M^{-1} \text{cm}^1$) ^a /nm | $\lambda_{\text{em}}^a/\text{nm}$ | $E_{\text{ox}}^b(\text{HOMO})/\text{V vs NHE}$ | E_{0-0}^c/eV | $E_{\text{red}}^b/\text{V vs NHE}$ | LUMO ^d /V vs NHE |
|-----------|--|-----------------------------------|--|-----------------------|------------------------------------|-----------------------------|
| P1 | 348 (34 720); 481 (57 900) | 618 | 1.32 | 2.25 | -0.83 | -0.93 |
| P2 | 337 (28 292); 404 (25 048); 531 (64 005) | 668 | 1.30 | 2.04 | -0.70 | -0.74 |
| P3 | 349 (27 140); 401 (22 530); 574 (40 990) | 783 | 1.40 | 1.86 | -0.36 | -0.46 |
| P7 | 302 (32 356); 357 (42 642); 490 (75 005) | 711 | 1.28 | 2.07 | -0.66 | -0.79 |

^a The absorption and emission spectra were measured in THF solution. The emission of **P3** was quite weak compared with other dyes. ^b The ground-state oxidation potential (E_{ox}) and reduction potential (E_{red}) of the dyes were measured in dry THF (**P2** and **P3**) and acetonitrile (**P1** and **P7**). ^c The 0–0 transition energy (E_{0-0}) was estimated from the intersection of normalized absorption and emission curves. ^d The LUMO energies were estimated from the oxidation potentials and E_{0-0} .

silver oxide. Finally, the intermediate **4**, upon treatment with tetracyanoethylene (TCNE) in DMF, gave the target dye **P3**.^{25,26}

Optical and Electrochemical Characterization. The UV–vis absorption spectra of the dyes, **P1**, **P2**, **P3**, and **P7**, in THF solution and adsorbed on NiO films are shown in Figure 2. For the UV–vis absorption spectra in THF solution, all the dyes exhibit one (or two) minor absorption band(s) and one prominent band, appearing at 300–420 and 400–700 nm, respectively, which are attributed to $\pi-\pi^*$ transitions of the conjugated chromophores. With a stronger electron-withdrawing group, the absorption spectra show a bathochromic shift of the maximum absorption, from 481 nm for **P1** to 574 nm for **P3**. By adsorbing the dyes on NiO film, a broadening of the absorption band is observed for all dyes, being attributed to the electronic coupling of the dye with the semiconductor surface and possibly some dye aggregation (see later section). Broadening of the dye absorption spectra on a metal oxide has previously been observed for coumarin sensitized NiO films¹⁵ as well as organic dyes on TiO₂ films.^{27,28} From the intersection of the normalized absorption and emission spectra, E_{0-0} energies of 2.25, 2.04, 1.86, and 2.07 eV were extracted for **P1**, **P2**, **P3** and **P7**, respectively.

The ground-state oxidation and reduction potentials of the dyes were measured by cyclic voltammetry (CV) in dry acetonitrile or THF containing 0.1 M TBA(PF₆) with 0.1 V s⁻¹ scan rate. As shown in Table 1, the oxidation potentials (approximately the HOMO levels) of the dyes range from 1.28 to 1.40 V vs NHE. These values are all much more positive than the valence band of NiO (~0.5 V vs NHE), so there should be a substantial driving force for hole injection from the dye to the semiconductor (Figure 3). The LUMO levels of these dyes can be estimated from the difference between E_{ox} and E_{0-0} and are in the range -0.46 to -0.93 V vs NHE. The reduction potentials of the dyes are also included in Table 1, and the values

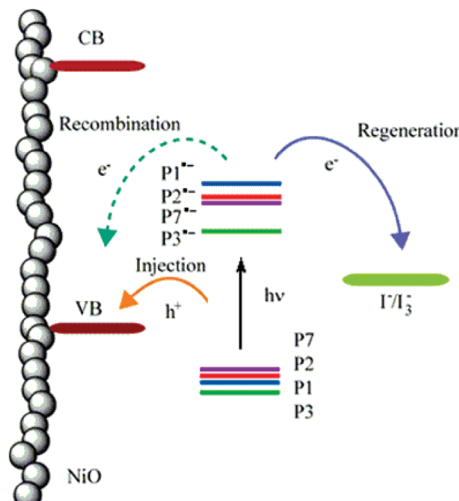


Figure 3. Schematic energy level diagram for p-type DSSCs.

measured are 0.04–0.13 V less negative than the estimated LUMO levels. It is clear that the electron-withdrawing groups have a big influence on the reduction potentials of the dyes and stronger electron-withdrawing ability corresponds to less negative reduction potential or lower lying LUMO energy. This will result in a lower thermodynamic driving force for dye regeneration. However, a stronger electron-withdrawing group should also improve the “push–pull” nature of the dye and increase the efficiency of charge separation within the molecule.

Anchoring of the Dyes on NiO. Infrared absorption spectra were measured for each of the dyes and sensitized NiO films in order to confirm the binding arrangement of the dye molecules to the substrate. Figure 4 shows the changes of the infrared absorption spectra of **P1**. In the vibrational spectrum of **P1** (Figure 4A), a split peak was observed assigned to the carbonyl

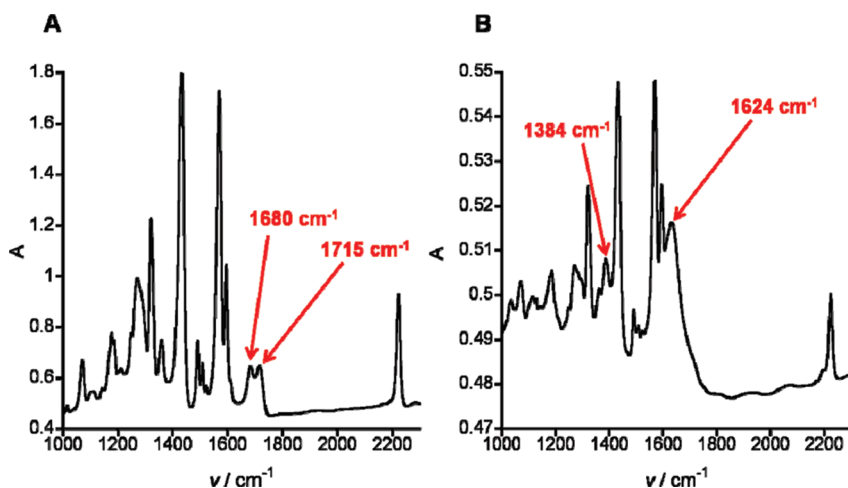


Figure 4. FTIR spectra of (A) **P1** and (B) **P1|NiO** (KBr pressed disk).

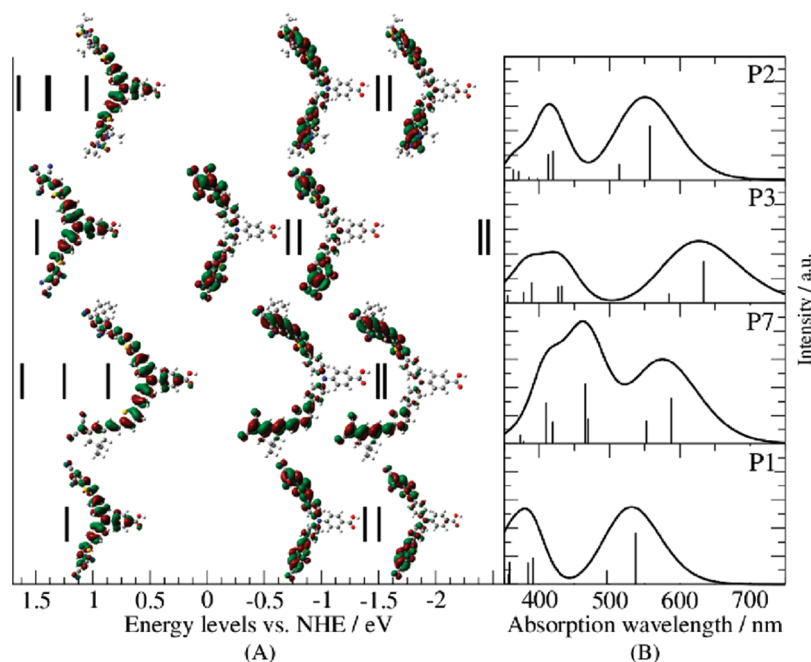


Figure 5. (A) Frontier orbital energy levels and isodensity plots of HOMO (left), LUMO (middle), and LUMO + 1 (right). (B) Time-dependent DFT gas phase spectra, generated from vertical transitions (displayed as black lines) by using an arbitrary 3000 cm⁻¹ Gaussian broadening.

stretching frequency. The splitting can be due to two possible hydrogen bonding geometries, with either one or two intermolecular hydrogen bonds, and is not present in the spectrum for the corresponding ester derivative (Table S1, Supporting Information).²⁹ The higher frequency peak was located at 1715 cm⁻¹, typical for a benzoic acid derivative measured in the solid state.³⁰ On adsorption on NiO (Figure 4B), the COO⁻ stretching frequency was lowered to 1624 cm⁻¹, assigned to the asymmetric stretch, and an additional signal at 1384 cm⁻¹ was present, corresponding to the symmetric stretch. This large difference between **P1** and **P1|NiO** is indicative of the binding of the dye to NiO surface via the carboxylic acid group.

For **P1**, no shift in frequency was observed for the C≡N stretch located at 2222 cm⁻¹, indicating that the cyano groups are not involved in binding to NiO. The key vibrational frequencies for each of the dyes, **P1**, **P2**, **P3**, and **P7**, and the equivalent sensitized films are listed in Table S1 in the Supporting Information. The spectra follow the same trend as described for **P1**, and therefore, we propose that all the dyes described here bind through the carboxylic acid group.

Time-Dependent (Hybrid) Density Functional Theory (DFT) Calculations. Hybrid-DFT calculations were employed to characterize the electronic structure of the chromophores. Optimization and vertical transitions were calculated at the B3LYP/6-31G(d)^{31–34} level, using Gaussian 03³⁵ as previously reported.⁵ The results are presented in Figure 5. Additional data are given in Table S2 in the Supporting Information. We noted that, although B3LYP is known to underestimate the energy of photoexcitation,³⁶ the calculated gas phase spectra compare well with the experimental data presented in Table 1. There is a discrepancy between the experimental and calculated spectra of **P7**, however. The latter spectrum has a very strong response in the blue region, due to multiple transitions, while the spectrum measured in THF is much narrow, similar to that of other dyes. This could be due to one or more transitions present in the gas phase being quenched in solution.

The isodensity plots confirm that the electronic structures are suitable for p-type sensitizers, since they shift electron density away from the anchor-donor moiety toward the acceptors. The two near-degenerate LUMOs observed are characteristic for this

TABLE 2: Photovoltaic Performance of DSSCs Based on P1, P2, P3, and P7^a

| | V_{oc} /mV | J_{sc} /mA cm ⁻² | ff | η /% | IPCE/% |
|-----------|--------------|-------------------------------|------|-----------|--------|
| P1 | 84 | 5.48 | 0.33 | 0.15 | 63 |
| P2 | 63 | 3.37 | 0.31 | 0.07 | 32 |
| P3 | 55 | 1.36 | 0.34 | 0.03 | 6 |
| P7 | 80 | 3.37 | 0.35 | 0.09 | 26 |

^a V_{oc} is the open-circuit voltage; J_{sc} is the short-circuit photocurrent density; ff is the fill factor; η is the overall conversion efficiency.

family of dyes. Because half of the LUMO + 1 possesses the same symmetry as the LUMO in all the cases, the HOMO → LUMO + 1 transition is partly allowed, giving rise to a weak transition approximately 50 nm shorter than the main HOMO → LUMO transition.

We further noted that the large red shift of **P3** is mainly due to the less negative LUMO level, while the calculated HOMO level is more positive than for other dyes, in accordance with the experimental observations. The other molecules have acceptor energy levels more similar to those of **P1**, illustrating that it is mainly the electron-withdrawing groups that dictate their positions.

p-Type Dye-Sensitized Solar Cells. The photovoltaic performance of solar cells based on these dyes is summarized in Table 2. Sandwich-type solar cells were assembled using **P1**-, **P2**-, **P3**-, and **P7**-sensitized nanocrystalline NiO as the working electrodes, platinized conducting glass as the counter electrode, and 1.0 M LiI, 0.1 M I₂ in acetonitrile, as the electrolyte. Figure 6 illustrates the incident monochromatic photon-to-current conversion efficiency (IPCE) spectra with these dyes. DSSC based on **P1** produced a maximum IPCE of 63%, whereas under the same conditions the devices based on **P2**, **P3**, and **P7** gave maximum IPCE values of 32%, 6%, and 26%, respectively. The solar cells based on **P2**, **P3**, and **P7** showed broadened IPCE spectra which matched the trend in absorption. The IPCE values are, however, much lower compared with that of the **P1**-sensitized device.

Under standard AM 1.5 sunlight irradiation (100 mW cm⁻²), the overall conversion efficiency of the **P1**-sensitized solar cell is the highest, followed by **P7** and **P2**. It is noted that, as the strength of the electron-withdrawing group increases, both the photovoltage and photocurrent decrease, especially for **P3**. The only difference in structure between **P1** and **P3** is that **P3** contains an extra cyano group on each acceptor arm compared to **P1**, whereas their photovoltaic properties are totally different. These results imply that the performance of solar cells may be influenced substantially by minor structural alterations of the dye.

II. Hole Injection. Spectroelectrochemistry. The properties of the radical anions of **P1** and **P3** were investigated by spectroelectrochemistry. They are chosen for comparison since they represent the highest and lowest energy conversion efficiencies, respectively, in this set of dyes. The absorption spectra of **P1|NiO** and **P3|NiO** films were recorded when scanning at 10 mV s⁻¹ between 0 and -1.5 V vs Fc/Fc⁺ for **P1|NiO** and -0.5 to -1.1 V vs Fc/Fc⁺ for **P3|NiO**. The reduction of **P1|NiO** was irreversible; the cathodic peak was located at -1.31 V vs Fc/Fc⁺ (-0.68 V vs NHE) and accompanied by decomposition of the dye. The reduction of **P3|NiO**, however, was reversible, located at -0.75 V vs Fc/Fc⁺ (-0.12 V vs NHE). Both these reduction potentials are located at approximately 200 mV less negative than those recorded in solution, in the presence of TBA(PF₆) supporting electrolyte. This trend has been observed in our laboratory for

other dyes, and it is thought that the Li⁺ cation helps to stabilize the dye radical anions.

The difference spectra of **P3|NiO** recorded while scanning to increasing negative potential is shown in Figure 7. The negative signal (bleach) corresponds to the neutral **P3|NiO**. The positive signal which grows in with time, centered at 500 nm, corresponds to **P3^{-|NiO}**. Since the reduction potential of the dye is located in the region of the band gap of the semiconductor, no electron transfer through the NiO is expected to occur.³⁷ A mechanism by which dyes may be reduced when adsorbed on the semiconductor substrate is electron transfer through the dye molecules. Since **P3** was easily reduced when adsorbed on the film, the dye molecules must be able to transfer electrons to each other very efficiently.

P1 was successfully reduced in acetonitrile solution. The difference spectra recorded when scanning from 0 to -1.7 V vs Fc/Fc⁺ are shown in Figure 8. The positive signals which grow in with time (increasing negative potential) correspond to **P1⁻**, and the bleach corresponds to the absorption of neutral **P1**.

Femtosecond Transient Absorption Measurements. Femtosecond transient absorption measurements were used to follow the formation and subsequent decay of the radical anions of the studied dyes. Measurements were made on **P1** and **P3** in both acetonitrile solution and adsorbed on NiO films.

In solution, **P1** and **P3** show decay kinetics with lifetimes around 30 and 3 ps, respectively. This is unusually fast for normal organic dyes. A potential reason for the short lifetimes is quenching of the excited states by dye-to-dye electron transfer. The spectral shape at 5 ps (Figure 9A) shows features that qualitatively resemble the sum of **P1⁻**, **P1⁺**, and the spectra of **P1** in solution at 0.5 ps. Also for **P3** there is a fast transition from the initial spectral shape (after 0.1 ps) to a spectral signature which in the blue part completely overlaps with the spectra of the **P3^{-|NiO}**. The buildup of signal around 700 nm is assigned to formation of **P3⁺**. As these dyes have clear charge transfer transitions, one would expect excited state absorption spectra similar to the sum of the reduced and oxidized species. However, as a transition with time is seen in Figure 9 which is not likely due to solvent relaxation, intermolecular electron transfer caused by aggregation is probable and supported by the fast kinetics.

In Figure 10, the transient spectrum of **P1|NiO** at 0.5 ps shows negative signals at wavelengths shorter than 550 nm due to the ground state bleach. Both the bleach and the peak at 610 nm of the broad positive absorption band, in the range of 575–770 nm, red shift in a few picoseconds. The red shift is probably due to solvent relaxation and/or other relaxation processes. The complexity of the spectral evolution, and thereby the species contributing to it, is signaled by the absence of any isosbestic points. However, the spectral shape correlates well with the sum of the spectra of **P1⁻** (Figure 8) and the broad absorption from 300 nm extending past 1100 nm of holes in NiO.³⁸

P3|NiO shows instant formation of a positive peak at 500 nm and a broad but weak positive band beyond 750 nm. The spectral shape is in good agreement with the signature of **P3^{-|NiO}** (Figure 7). The ground state bleaching is also broad and structureless in correlation with the absorption spectrum of the adsorbed dye, though the Rayleigh scattering from the pump beam covers the expected peak at 580 nm. The spectral shape is constant through the measured time interval, from 0 to 1.5 ns.

From spectroelectrochemistry measurements, *vide supra*, radical formation and decay were studied at 620 nm for **P1|NiO**

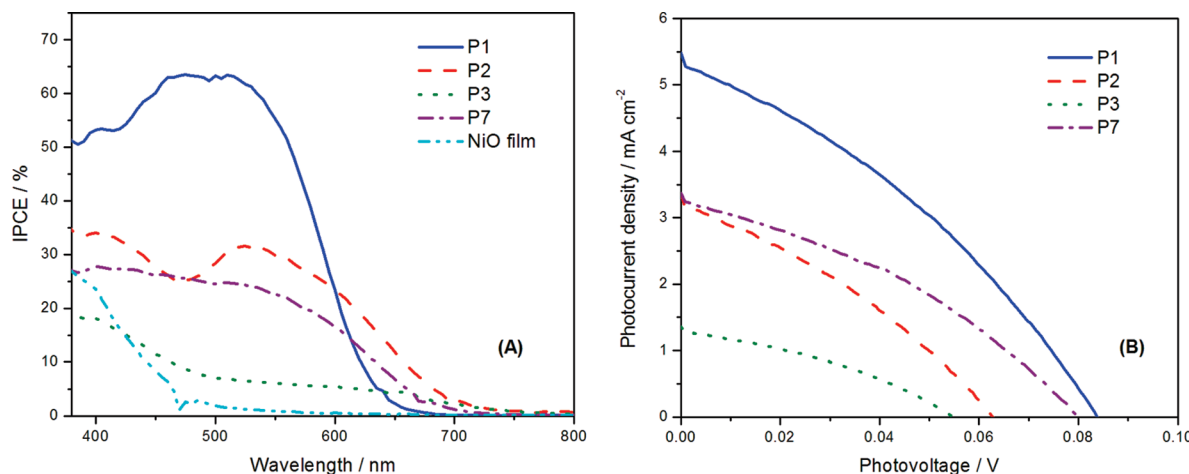


Figure 6. Comparison of IPCE spectra (A) and current–voltage characteristics (B) of **P1**-, **P2**-, **P3**-, and **P7**-sensitized NiO solar cells under AM 1.5G (100 mW cm^{-2}) illumination.

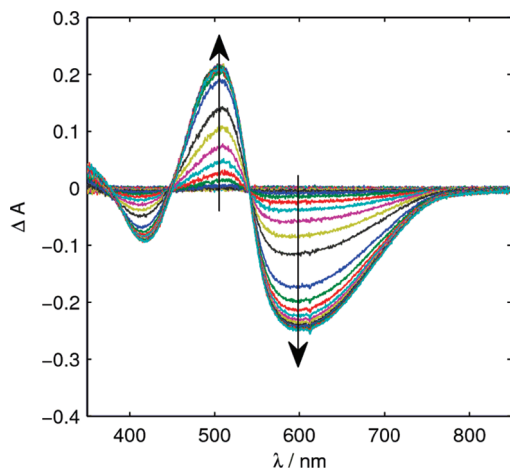


Figure 7. Spectral changes recorded upon electrolytic reduction of **P3|NiO** in acetonitrile with 0.1 M LiClO₄. The arrows indicate the observed changes.

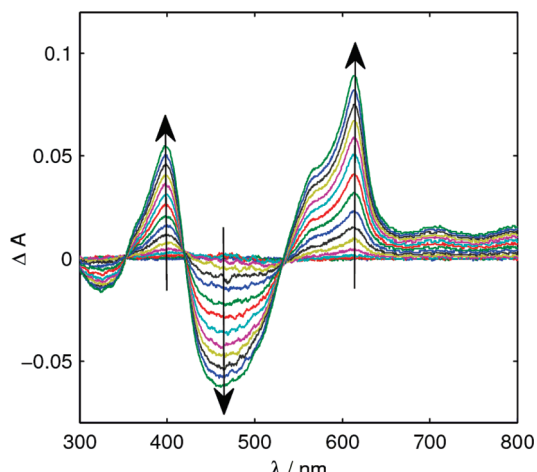


Figure 8. Spectral changes recorded upon electrolytic reduction of **P1** in acetonitrile solution with 0.1 M LiClO₄. The arrows indicate the changes observed.

and at 500 nm for **P3|NiO**. The maximum ΔA signal was 0.012 and 0.017 at the probe wavelength for **P1|NiO** and **P3|NiO**, respectively, although normalized for clarity in Figure 11. The transient decays were fitted with a sum of exponentials and deconvoluted with a Gaussian shaped pump–probe correlation function, giving the lifetimes presented in Table 3.

P3|NiO has a pulse width limited signal rise, which is different from **P1|NiO**, where the transient absorption signal clearly needs a rise time component. For both dyes, the subsequent decay lifetimes are quite similar with components of 2–3 ps, ~20 ps, and 200–300 ps of different amplitudes, which are ascribed to fast recombination. There is also, for both **P1|NiO** and **P3|NiO**, at least one long-lived decay component is present.

The fast injection and recombination is in agreement with transient absorption studies on other p-type systems. Coumarin 343 on NiO, for example, has an injection rate corresponding to <200 fs and a recombination rate of $(20 \text{ ps})^{-1}$.¹⁵ The same trend has also been observed for other p-type dyes such as a peryleneimide dye⁶ and porphyrins.¹⁸ Also, corresponding to work on both n-type and p-type dyes, a correlation between the energy conversion efficiency of the cell and the amount of long-lived radicals is expected.³⁹ **P3**, which is the least efficient dye in this series, has an IPCE value of only 6% and was anticipated to have either low hole injection probability or an inefficient dye regeneration.

As the excited state lifetime of **P3** in acetonitrile is only 3 ps, albeit at high concentrations with a substantial probability of aggregate formation, the injection probability of this dye could be highly compromised, especially since **P3** seems prone to **P3–P3** electron transfer. On the other hand, the rise of the transient absorption signal is immediate (<150 fs), which, in spite of the short excited state lifetime, corresponds to an injection efficiency of more than 90%. For **P1|NiO**, there is a rise of about 200 fs in comparison to **P3|NiO** for which the signal buildup is pulse width limited, indicating a faster hole injection for **P3** than **P1**. The extra cyano group in the electron acceptor part of **P3** appears to shift the charge transfer state to lower energy and might thereby impose a more distinct excited state charge transfer character. Moreover, because the HOMO level of **P3** is lower in energy, there is also a higher driving force for hole injection for **P3** than for **P1**, which should also give faster injection in the **P3|NiO** system.

The proportion of radical species remaining after 1.5 ns is higher for **P3|NiO** than for **P1|NiO**, but values of η and IPCE are lower for **P3** than for **P1**, which indicates rather low regeneration efficiency for **P3**. It should be noted, though, that the IPCE is measured at short circuit, which could alter the kinetics in the system compared to the open circuit conditions that were employed in these measurements. Since there seems to be no problem with the charge separation mechanism for

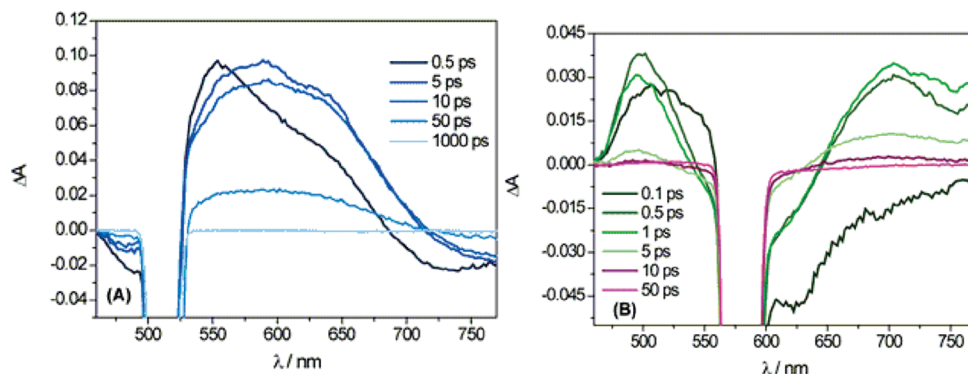


Figure 9. Transient absorption spectra of (A) **P1** and (B) **P3** in acetonitrile after excitation at 510 and 575 nm, respectively. The strong Rayleigh scattering at the excitation wavelength has been omitted.

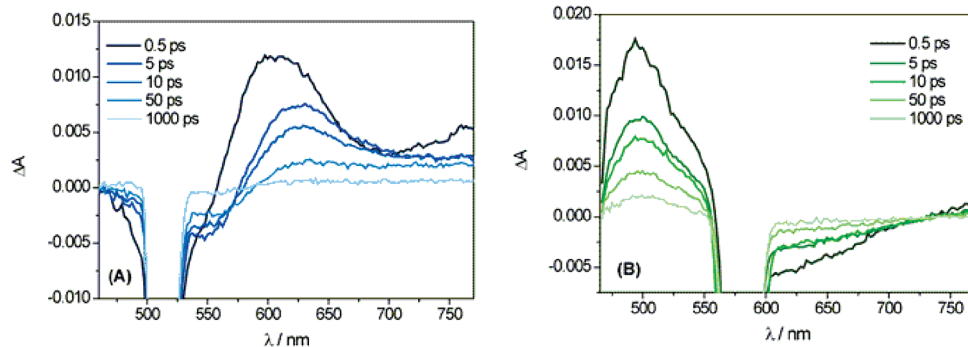


Figure 10. Transient absorption spectra of (A) **P1|NiO** and (B) **P3|NiO** in the presence of 1.0 M LiClO₄ in acetonitrile.

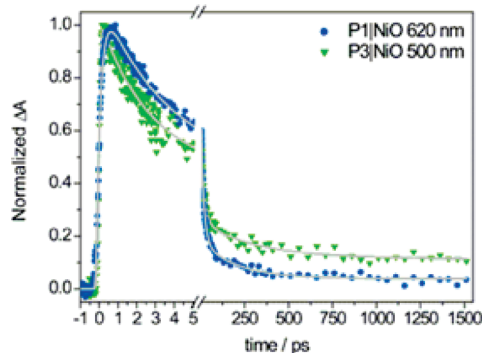


Figure 11. Transient absorption decay traces of **P1|NiO** (blue dots) and **P3|NiO** (green triangles), along with exponential fits (gray lines). The excitation was at 510 nm/575 nm for **P1/P3**, probing at 620 nm/500 nm.

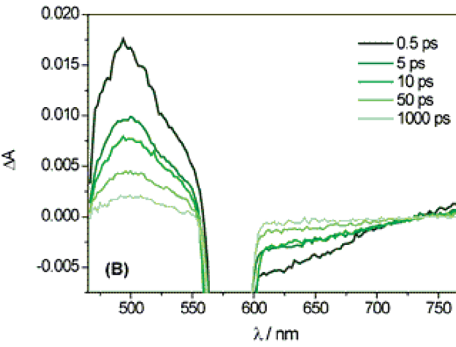
TABLE 3: Fitted Lifetimes with Corresponding Amplitudes for P1 and P3

| τ_1 (injection) | τ_2 | τ_3 | τ_4 | y_0^a |
|----------------------|------------------|-------------|------------|-------------|
| P1 NiO | 230 fs, 50% rise | 2.7 ps, 20% | 17 ps, 22% | 205 ps, 6% |
| P3 NiO | <200 fs | 2.4 ps, 48% | 20 ps, 28% | 317 ps, 13% |

^a An extra exponential with a fixed lifetime of 30 ns was used to cover the amplitude of any long-lived signal.

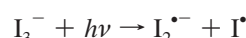
either dye, and in fact, **P3** appears to be a better sensitizer than **P1** for NiO, we next investigated the dye regeneration processes.

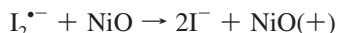
Indications of Dye Aggregation. The short excited state lifetime of both **P1** and **P3** is in agreement with the low emission quantum yield observed in acetonitrile solution. In THF, the quantum yield for emission for **P1** is increased over 200 times compared to in acetonitrile, while **P3** has weak emission in THF and is completely nonemissive in acetonitrile. Moreover, the location of the absorption peak of **P3** was shown to be concentration dependent (Figure S2, Supporting Information).



These are strong indications for solvent dependent dye aggregation. **P3** is assumed to have the strongest tendency to aggregate due to the increased broadening of the main absorption peak when adsorbed on NiO compared to the other dyes, and due to its efficient dye–dye electron transfer properties, described in the previous section. The calculations and absorption spectra also show that this dye has the strongest push–pull effect, which could give an increased tendency for aggregation and intermolecular electron transfer.

III. Dye Regeneration. Photoinduced Absorption Spectroscopy (PIA). Photoinduced absorption spectroscopy in the presence of redox electrolyte was performed to compare the dye regeneration efficiency of **P1** vs **P3**. Both dyes were excited at a wavelength close to their absorption maxima in the visible region: **P1|NiO** was excited at 460 nm using a blue diode and **P3|NiO** was excited at 630 nm using a red diode laser, at a modulation frequency of 9.33 Hz. **P1|NiO** and **P3|NiO** samples were optically matched at the excitation wavelength to get a good indication of the relative efficiency of the process from the intensity of the signal. The transient absorption spectrum of the sensitized film was measured first in the absence of redox electrolyte, and in agreement with the ultrafast experiments, no signal was observed suggesting that all the processes were complete within this time scale (minimum of microseconds). The transient absorption spectra of the unsensitized NiO and sensitized films in the presence of the redox electrolyte are shown in Figure 12. For the unsensitized NiO film, on excitation at 460 nm a small, featureless, positive signal was observed in the difference spectrum, corresponding to holes in the NiO created by the photoreaction with the I₃⁻ in the electrolyte:¹⁴

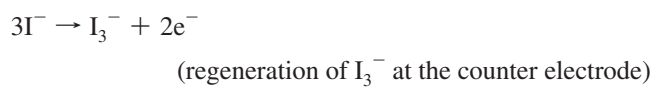
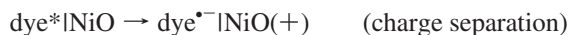




On excitation at 630 nm, no signal was observed. These observations were in agreement with the IPCE spectrum of unsensitized NiO film, which has a photocurrent at 460 nm but no response at 630 nm.

The PIA spectra of the sensitized films in the presence of electrolyte are notably different. For **P1|NiO**, an intense, positive signal was observed, corresponding to the holes injected into NiO from the dye (with presumably a relatively small contribution from the electrolyte). For **P3|NiO**, the transient absorption spectrum matched that of the unsensitized film excited at the same wavelength and there was negligible signal. This suggests that **P1** is efficiently regenerated by the electrolyte, whereas **P3** is not.

Mechanism of Dye Regeneration. On the basis of the above results and the former studies,^{2,3,15,18} the following mechanism can be proposed:



Upon excitation of the dye, charge separation occurs. A hole is injected into the NiO valence band, and the dye is reduced. The reduced dye will react with the oxidized species (I_3^-) of the electrolyte and regenerate to its ground state. In this case, $\text{I}_2^{\bullet-}$ would be generated, which is also a common intermediate

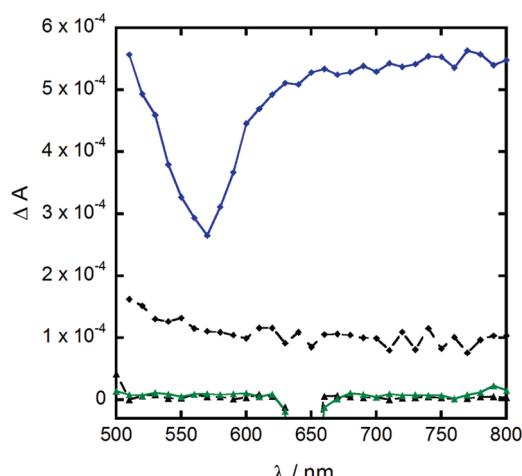


Figure 12. Plot of photoinduced absorption of unsensitized NiO (black), **P1|NiO** (blue), and **P3|NiO** (green) in the presence of 1.0 M LiI, 0.1 M I_2 in acetonitrile, and excited at 460 nm (diamonds) and 630 nm (triangles).

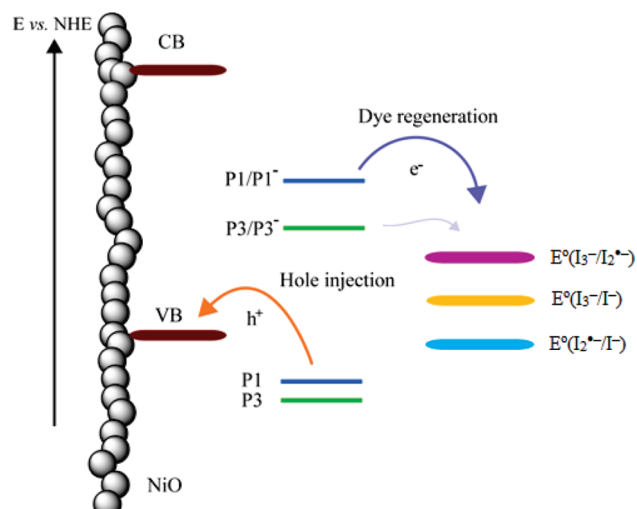


Figure 13. Schematic energy level diagram for **P1** and **P3**.

in TiO_2 based solar cells.^{40,41} If the dye radical anion does not react with the redox couple within the lifetime of the charge-separated state, the reduced dye could also be reoxidized by the hole in the semiconductor, i.e., by geminate recombination. The presence of the $\text{I}_2^{\bullet-}$ intermediate has been observed by photoinduced absorption spectroscopy¹⁴ and can take part in a number of reactions including with the NiO to give a second hole, or disproportionation. The triiodide is regenerated at the counter electrode, completing the cycle.

Wang and Stanbury reported an upper limit of 0.30 V vs Fc/Fc⁺ (0.93 V vs NHE) for $E^\circ(\text{I}_2^{\bullet-}/\text{I}^-)$.⁴² $E^\circ(\text{I}_3^-/\text{I}_2^{\bullet-})$ and $E^\circ(\text{I}_2^{\bullet-}/\text{I}^-)$ should lie symmetrically around $E^\circ(\text{I}_3^-/\text{I}^-)$, giving $E^\circ(\text{I}_3^-/\text{I}_2^{\bullet-})$ at approximately -0.35 V vs NHE.⁴³ The driving force (Gibbs free energy difference) for the oxidation of the dye radical anion by I_3^- (i.e., the dye regeneration reaction) is the difference between the reduction potential of the dye and the one electron reduction potential of I_3^- . Figure 13 shows an energy level diagram that compares the relative positions of the components in the p-type DSSC. From the relative energy levels, there is sufficient driving force for regeneration of **P1** by I_3^- , but insufficient driving force for regeneration of **P3**. While the values are estimates, these figures explain the inability of the triiodide–iodide redox couple to regenerate **P3** and the corresponding low performance of the **P3**-sensitized NiO DSSC.

Dark Current Measurement. As mentioned in part II, the short lifetime of the charge-separated state for the **P1** dye was surprising considering the apparently high efficiency of regeneration by the redox mediator. One explanation for the apparently fast regeneration process could be the existence of some preassociated dye–triiodide species. It has been proposed that some organic dyes used in n-type DSSCs show an increased tendency for recombination between electrons in the TiO_2 conduction band and the oxidized redox mediator due to association of the redox species, e.g., I_2 or I_3^- , with the dye.⁴⁴ In such examples an increase of the dark current has been observed. While this is unfavorable in n-type devices, it may be of benefit in p-type DSSCs where fast recombination between the dye radical anion and holes in the NiO competes with the diffusion of the redox mediator and regeneration of the neutral, ground state dye.¹⁵ To test this hypothesis, sandwich cells were fabricated using **P1**- and **P3**-sensitized TiO_2 and infiltrated with the same I^-/I_3^- electrolyte as for the p-type devices. The 6.5 μm thick TiO_2 films were prepared from basic ECN paste⁴⁵ with an active area of 0.48 cm^2 . After soaking in 0.3 mM dye solution in acetonitrile (**P1**) or 20:1 acetonitrile:DMF (**P3**) for

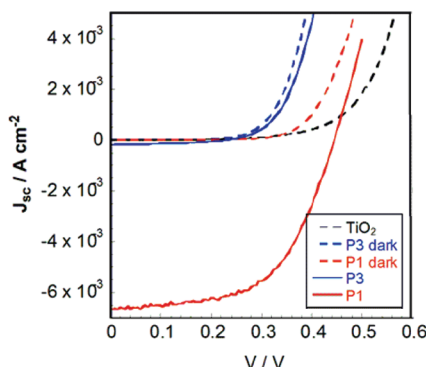


Figure 14. Light and dark current–voltage characteristics of TiO_2 -based DSSCs sensitized with **P1** and **P3**.

16 h at room temperature, the cells were assembled. A sandwich cell with unsensitized TiO_2 was also assembled for comparison.

$J-V$ characteristics on illumination with 100 mW cm^{-2} light and in the dark are shown in Figure 14. **P1** functions reasonably well as a photosensitizer for TiO_2 , generating a short-circuit photocurrent of 6.65 mA cm^{-2} , whereas **P3** does not. This can be attributed to the LUMO energy level of **P1** lying above, and the LUMO energy level of **P3** lying below, the conduction band of TiO_2 . The dark currents are shown as dashed lines, and from Figure 14 it is apparent that the dark current is higher for **P3**, followed by **P1**, and then bare TiO_2 . One explanation could be the location of I_3^- close to the TiO_2 surface by association with the dye molecules. This is in agreement with our suggestion that I_3^- is preassociated with the dyes, ready to intercept the charge on the photogenerated dye radical anion.

Conclusion

We have designed and synthesized a series of triphenylamine-based chromophores and investigated the effect of electron-withdrawing groups on the photophysical and electrochemical properties, as well as the photovoltaic performance of the dyes. By using different electron-withdrawing groups, the energy levels are tuned and this has a large influence on the hole injection and dye regeneration processes.

Femtosecond transient absorption spectroscopy of **P1** and **P3** adsorbed on the NiO films revealed an injection rate for both dyes of more than $(250 \text{ fs})^{-1}$. Although the excited state lifetimes of these dyes are less than 30 ps, such fast injection corresponds to more than 90% injection efficiency for both dyes. The subsequent recombination gave amplitudes of long-lived radical states ($>2 \text{ ns}$) corresponding to only 2% and 12% for **P1** and **P3**, respectively. The PIA spectra of the sensitized film in the presence of electrolyte showed efficient ground-state dye regeneration for **P1**, but poor regeneration for **P3**. The latter is caused by the location of the reduction potential of **P3** relative to the $\text{I}_3^-/\text{I}_2^\cdot-$ energy level, which results in insufficient driving force for oxidation of the dye radical anion by I_3^- . The fast regeneration for **P1** is explained by association of I_3^- with the dye *prior* to excitation and charge injection to NiO . It is postulated that the overall conversion efficiency of **P3** could be improved by substituting the I_3^-/I^- electrolyte for a one-electron, outer-sphere mediator with a redox potential matched to the NiO valence band and reduction potential of the dye.

Acknowledgment. This work was supported by the Swedish Research Council, the Swedish Energy Agency, the Knut and Alice Wallenberg Foundation, and the China Scholarship Council (CSC). We thank Dr. Yan Gao (Stockholm Univer-

sity) for the HRMS measurements and Ute B. Cappel (Uppsala University) for assisting with spectroelectrochemistry measurements.

Supporting Information Available: Table of key infrared frequencies of the dyes and sensitized films; the transient absorption decay of **P1** and **P3** in acetonitrile solution; the absorption spectra of **P3** in acetonitrile solution with different concentration and calculation details. This material is available free of charge via the Internet at <http://pubs.acs.org>.

References and Notes

- Mori, S.; Fukuda, S.; Sumikura, S.; Takeda, Y.; Tamaki, Y.; Suzuki, E.; Abe, T. *J. Phys. Chem. C* **2008**, *112*, 16134–16139.
- Morandeira, A.; Fortage, J.; Edvinsson, T.; Pleux, L. L.; Blart, E.; Boschloo, G.; Hagfeldt, A.; Hammarström, L.; Odobel, F. *J. Phys. Chem. C* **2008**, *112*, 1721–1728.
- Morandeira, A.; Boschloo, G.; Hagfeldt, A.; Hammarström, L. *J. Phys. Chem. C* **2008**, *112*, 9530–9537.
- Qin, P.; Zhu, H.; Edvinsson, T.; Boschloo, G.; Hagfeldt, A.; Sun, L. *J. Am. Chem. Soc.* **2008**, *130*, 8570–8571.
- Qin, P.; Linder, M.; Brinck, T.; Boschloo, G.; Hagfeldt, A.; Sun, L. *Adv. Mater.* **2009**, *21*, 2993–2996.
- Gibson, E. A.; Smeigh, A. L.; Pleux, L. L.; Fortage, J.; Boschloo, G.; Blart, E.; Pellegrin, Y.; Odobel, F.; Hagfeldt, A.; Hammarström, L. *Angew. Chem., Int. Ed.* **2009**, *48*, 4402–4405.
- Nakasa, A.; Usami, H.; Sumikura, S.; Hasegawa, S.; Koyama, T.; Suzuki, E. *Chem. Lett.* **2005**, *34*, 500–501.
- He, J.; Lindström, H.; Hagfeldt, A.; Lindquist, S.-E. *Sol. Energy Mater. Sol. Cells* **2000**, *62*, 265–273.
- O'Regan, B.; Grätzel, M. *Nature* **1991**, *353*, 737–740.
- Hagfeldt, A.; Grätzel, M. *Acc. Chem. Res.* **2000**, *33*, 269–277.
- Nazeeruddin, M. K.; De Angelis, F.; Fantacci, S.; Selloni, A.; Viscardi, G.; Liska, P.; Ito, S.; Takeru, B.; Grätzel, M. *J. Am. Chem. Soc.* **2005**, *127*, 16835–16847.
- Chiba, Y.; Islam, A.; Watanabe, Y.; Komiya, R.; Koide, N.; Han, L. *Jpn. J. Appl. Phys.* **2006**, *45*, L638–L640.
- Mizoguchi, Y.; Fujihara, S. *Electrochem. Solid-State Lett.* **2008**, *11*, 78–80.
- Zhu, H.; Hagfeldt, A.; Boschloo, G. *J. Phys. Chem. C* **2007**, *111*, 17455–17458.
- Morandeira, A.; Boschloo, G.; Hagfeldt, A.; Hammarström, L. *J. Phys. Chem. B* **2005**, *109*, 19403–19410.
- Vera, F.; Schrebler, R.; Muñoz, E.; Suarez, C.; Cury, P.; Gómez, H.; Córdova, R.; Marotti, R. E.; Dalchiele, E. A. *Thin Solid Films* **2005**, *490*, 182–188.
- He, J.; Lindström, H.; Hagfeldt, A.; Lindquist, S.-E. *J. Phys. Chem. B* **1999**, *103*, 8940–8943.
- Borgström, M.; Blart, E.; Boschloo, G.; Mukhtar, E.; Hagfeldt, A.; Hammarström, L.; Odobel, F. *J. Phys. Chem. B* **2005**, *109*, 22928–22934.
- Pettersson, K.; Wikberg, J.; Ljungdahl, T.; Mårtensson, J.; Albinsson, B. *J. Phys. Chem. A* **2006**, *110*, 319–326.
- Sumikura, S.; Mori, S.; Shimizu, S.; Usami, H.; Suzuki, E. *J. Photochem. Photobiol. A: Chem.* **2008**, *199*, 1–7.
- Li, L.; Gibson, E. A.; Qin, P.; Boschloo, G.; Gorlov, M.; Hagfeldt, A.; Sun, L. *Adv. Mater.* [Online early access]. DOI: 10.1002/adma.200903151. Published Online: Jan 13, 2010.
- Koeckelberghs, G.; Vangheluwe, M.; Picard, I.; De Groof, L.; Verbiest, T.; Persoons, A.; Samyn, C. *Macromolecules* **2004**, *37*, 8530–8537.
- Leriche, P.; Frère, P.; Cravino, A.; Alévêque, O.; Roncali, J. *J. Org. Chem.* **2007**, *72*, 8332–8336.
- Melucci, M.; Barbarella, G.; Zambianchi, M.; Di Pietro, P.; Bongini, A. *J. Org. Chem.* **2004**, *69*, 4821–4828.
- Spraul, B. K.; Suresh, S.; Sassa, T.; Ángeles Herranz, M.; Echegoyen, L.; Wada, T.; Perahia, D.; Smith, D. W., Jr. *Tetrahedron Lett.* **2004**, *45*, 3253–3256.
- McKusick, B. C.; Heckert, R. E.; Cairns, T. L.; Coffman, D. D.; Mower, H. F. *J. Am. Chem. Soc.* **1958**, *80*, 2806–2815.
- Li, G.; Jiang, K.; Li, Y.; Li, S.; Yang, L. *J. Phys. Chem. C* **2008**, *112*, 11591–11599.
- Horiuchi, T.; Miura, H.; Sumioka, K.; Uchida, S. *J. Am. Chem. Soc.* **2004**, *126*, 12218–12219.
- Reva, I. D.; Stepanian, S. G. *J. Mol. Struct.* **1995**, *349*, 337–340.
- Deacon, G. B.; Phillips, R. J. *Coord. Chem. Rev.* **1980**, *33*, 227–250.
- Becke, A. D. *Phys. Rev. A* **1988**, *38*, 3098–3100.
- Becke, A. D. *J. Chem. Phys.* **1993**, *98*, 1372–1377.
- Lee, C.; Yang, W.; Parr, R. G. *Phys. Rev. B* **1988**, *37*, 785–789.

- (34) Hehre, W. J.; Ditchfield, R.; Pople, J. A. *J. Chem. Phys.* **1972**, *56*, 2257–2261.
- (35) Frisch, M. J.; Trucks, G. W.; Schlegel, H. B.; Scuseria, G. E.; Robb, M. A.; Cheeseman, J. R.; Montgomery, J. A., Jr.; Vreven, T.; Kudin, K. N.; Burant, J. C.; Millam, J. M.; Iyengar, S. S.; Tomasi, J.; Barone, V.; Mennucci, B.; Cossi, M.; Scalmani, G.; Rega, N.; Petersson, G. A.; Nakatsuji, H.; Hada, M.; Ehara, M.; Toyota, K.; Fukuda, R.; Hasegawa, J.; Ishida, M.; Nakajima, T.; Honda, Y.; Kitao, O.; Nakai, H.; Klene, M.; Li, X.; Knox, J. E.; Hratchian, H. P.; Cross, J. B.; Adamo, C.; Jaramillo, J.; Gomperts, R.; Stratmann, R. E.; Yazev, O.; Austin, A. J.; Cammi, R.; Pomelli, C.; Ochterski, J. W.; Ayala, P. Y.; Morokuma, K.; Voth, G. A.; Salvador, P.; Dannenberg, J. J.; Zakrzewski, V. G.; Dapprich, S.; Daniels, A. D.; Strain, M. C.; Farkas, O.; Malick, D. K.; Rabuck, A. D.; Raghavachari, K.; Foresman, J. B.; Ortiz, J. V.; Cui, Q.; Baboul, A. G.; Clifford, S.; Cioslowski, J.; Stefanov, B. B.; Liu, G.; Liashenko, A.; Piskorz, P.; Komaromi, I.; Martin, R. L.; Fox, D. J.; Keith, T.; Al-Laham, M. A.; Peng, C. Y.; Nanayakkara, A.; Challacombe, M.; Gill, P. M. W.; Johnson, B.; Chen, W.; Wong, M. W.; Gonzalez, C.; Pople, J. A. *Gaussian 03*, revision C.02; Gaussian, Inc.: Pittsburgh, PA, 2003.
- (36) Dreuw, A.; Head-Gordon, M. *Chem. Rev.* **2005**, *105*, 4009–4037.
- (37) Cappel, U. B.; Gibson, E. A.; Hagfeldt, A.; Boschloo, G. *J. Phys. Chem. C* **2009**, *113*, 6275–6281.
- (38) Boschloo, G.; Hagfeldt, A. *J. Phys. Chem. B* **2001**, *105*, 3039–3044.
- (39) Wiberg, J.; Marinado, T.; Hagberg, D. P.; Sun, L.; Hagfeldt, A.; Albinsson, B. *J. Phys. Chem. C* **2009**, *113*, 3881–3886.
- (40) Bauer, C.; Boschloo, G.; Mukhtar, E.; Hagfeldt, A. *J. Phys. Chem. B* **2002**, *106*, 12693–12704.
- (41) Peter, L. M. *J. Phys. Chem. C* **2007**, *111*, 6601–6612.
- (42) Wang, X.; Stanbury, D. M. *Inorg. Chem.* **2006**, *45*, 3415–3423.
- (43) Boschloo, G.; Hagfeldt, A. *Acc. Chem. Res.* **2009**, *42*, 1819–1826.
- (44) O'Regan, B. C.; López-Duarte, I.; Martínez-Díaz, M. V.; Forneli, A.; Albero, J.; Morandeira, A.; Palomares, E.; Torres, T.; Durrant, J. R. *J. Am. Chem. Soc.* **2008**, *130*, 2906–2907.
- (45) Pettersson, H.; Gruszecki, T.; Bernhard, R.; Häggman, L.; Gorlov, M.; Boschloo, G.; Edvinsson, T.; Kloof, L.; Hagfeldt, A. *Prog. Photovoltaics: Res. Appl.* **2007**, *15*, 113–121.

JP911091N